Mon. Not. R. astr. Soc. (1987) **224,** 13–39

A completely analytical family of anisotropic Plummer models

Herwig Dejonghe *School of Natural Sciences, Institute for Advanced Study, Princeton, NJ 08540, USA*

Accepted 1986 June 11. Received 1986 June 10; in original form 1986 March 24

Summary. In spherical stellar systems, a given mass density allows an infinity of distribution functions. This indeterminacy is illustrated with a one-parameter family of anisotropic models. They all satisfy the Plummer law in the mass density, but have different velocity dispersions. Moreover, the stars are not confined to a particular subset of the total accessible phase space. This family is explored analytically in detail (the moments, various energy distributions, the line profiles can all be calculated). Even when both the mass density and the velocity dispersion profiles are required to be the same, a degeneracy in the model space persists, which can be shown with a three-parameter generalization of the above family. The observational consequence of the degeneracy are studied by calculating the observable line profiles obtained with different distribution functions. This provides an estimate of the accuracy needed in the observed shape of the line profiles in order to be of use in the determination of the distribution function.

1 Introduction

We can subdivide roughly the study of a stellar system into two major parts. The first concerns the determination of the shape of the system. The central problem is to retrieve three-dimensional information from our two-dimensional viewpoint. This deprojection problem becomes increasingly more tricky when more detailed observations reveal irregularities and suggest more general shapes or more physical quantities which are to be taken into account. In the mid-70s there was considerable discussion as to whether axisymmetric elliptical systems were predominantly oblate or prolate. Without being satisfactorily resolved, this discussion triggered the recognition that a considerable fraction of the regular ellipticals were actually triaxial (Binney 1978; de Zeeuw 1985)! It is assumed here that it still makes sense to think of detailed observations of astronomical objects which may be interpreted within the framework of an essentially spherical geometry. Within this hypothesis of sphericity, the deprojection is not a mathematical difficulty. It is further on always assumed that we can dispose of properly deprojected spherical three-dimensional physical quantities as a function of the spherical radius r.

Nowadays, a complete set of observations includes also measurements of the velocity

dispersions of the stars. As we are then digging deeper into the structure of the system, the reduction of these data requires more explicit dynamical assumptions. This is typical of the second stage in the modelling scheme, in which we try to interpret the observations on a more fundamental level with dynamical statements. For classical collisionless stellar systems, the best and the ultimate we can do is the determination of the distribution function in phase space, i.e. the probability of finding a star at a given position and with a given velocity (also called the fundamental problem of stellar dynamics).

The purposes of the present paper are mainly twofold. First, after summarizing the relevant formulae that connect the internal dynamics and the observable quantities for spherical systems in Section 2, we present in Section 3 in considerable detail a special family of spherical models, based upon the Plummer (1911) model. All the members of the family have the same Plummer density law, but the orbital structure varies. In particular, this is seen in the velocity-dispersion profiles and marginal distributions which can be calculated analytically. Moreover, all the moments of the line-of-sight velocity distribution at a particular radius can be given explicitly. Though high-order moments are difficult to interpet, they enable us to calculate the line profiles with considerable accuracy. Secondly, we elaborate in the observational consequences of the indeterminacy in the compatible distribution functions. If we assume properly determined mass density and velocity dispersions (Binney & Mamon 1982), we show in Section 4 with the aid of some explicit examples (of the Plummer family) that the mass density and velocity dispersions are not sufficient to reconstruct the distribution function. It is possible to calculate the effect of the degeneracy in the compatible distribution functions on the observable line profiles. In this respect, this paper is complementary to the work by Richstone & Tremaine (1984), who assess by numerical means the freedom in mass-to-light ratio, given a single velocity-dispersion measurement at some radius. Here, in contrast, both the mass density and the velocity-dispersion profile are fixed, and the work is carried out almost completely analytically.

2 Some general formulae

2.1 THE ISOTROPIC SPHERICAL CLUSTER

In the isotropic case, the velocity dispersions in spherical coordinates σ_r, σ_φ, σ_θ are all equal. In phase space, the distribution function $F_E(E) \equiv F(E)$ is function of the binding energy per unit mass E only, where

$$E = \psi(r) - \tfrac{1}{2}(v_r^2 + v_\varphi^2 + v_\theta^2) \tag{1}$$

is the most important (and generally the only) isolating integral of the equations of motion in a time-independent potential. The function $\psi(r) \geq 0$ is the potential of the system, connected with the mass density $\varrho(r)$ through the equation of Poisson:

$$\frac{1}{r^2} D_r[(r^2 D_r \psi(r)] = -4\pi G \varrho(r) \tag{2}$$

with G the gravitational constant, and D_r denotes differentiation with respect to r. The connection between $F(E)$ and $\varrho(r)$ is given by

$$\varrho(\psi) = 4\pi M \int_0^\psi F(E) \sqrt{2(\psi - E)}\, dE \tag{3}$$

with M the total mass. The fundamental integral equation (3) was first solved by Eddington (1916):

$$F(E) = \frac{1}{2\pi^2 M} D_E^2 \int_0^E \frac{\varrho(\psi)\, d\psi}{\sqrt{2(E - \psi)}}. \tag{4}$$

It should be noted that we need $\varrho(\psi)$ instead of $\varrho(r)$, which is an important difficulty in the analytical construction of isotropic models (Dejonghe 1984).

The velocity dispersions are

$$\sigma^2(\psi)=\sigma_r^2(\psi)=\sigma_\varphi^2(\psi)=\sigma_\theta^2(\psi)=\frac{1}{\varrho(\psi)}\int_0^\psi \varrho(\psi')\,d\psi', \tag{5}$$

and the fourth moments are

$$\tfrac{1}{3}\tau_{rr}^4=\tfrac{1}{3}\tau_{\varphi\varphi}^4=\tfrac{1}{3}\tau_{\theta\theta}^4=\tau_{r\varphi}^4=\tau_{r\theta}^4=\tau_{\theta\varphi}^4=\frac{1}{\varrho(\psi)}\int_0^\psi(\psi-\psi')\,\varrho(\psi')\,d\psi'. \tag{6}$$

We can conclude the isotropic case with the remark that the mass density (or in general one moment of the distribution function) suffices to determine $F(E)$. The fundamental problem has therefore a unique solution.

2.2 THE ANISOTROPIC SPHERICAL CLUSTER

In the so-called anisotropic case, the distribution function depends on a second isolating integral

$$L=r\sqrt{v_\varphi^2+v_\theta^2}=rv_\mathrm{T}, \tag{7}$$

which is the modulus of the angular momentum vector.

The dispersions σ_φ and σ_θ are equal, but differ from σ_r. The fundamental integral equation that relates the distribution function $F_{\mathrm{E,L}}(E, L)\equiv F(E, L)$ to the mass density now reads

$$\varrho(\psi, r)=2\pi M\int_0^\psi dE\int_0^{2(\psi-E)}\frac{F(E, L)}{\sqrt{2(\psi-E)-v_\mathrm{T}^2}}\,dv_\mathrm{T}^2. \tag{8}$$

In contrast to the isotropic case, the double integration over the distribution function gives the mass density as a function of the potential ψ and the spherical radius r. It is immediately apparent that different $F(E, L)$ usually lead to different $\varrho(\psi, r)$ but not necessarily to different $\varrho(r)=\varrho(\psi(r), r)$. Essentially, the problem comes to the necessity of knowing the full $\varrho(\psi, r)$, while we have only the cut $\varrho(\psi(r), r)$, provided by the observation of the mass density. We instead need infinitely many cuts, at least in principle. This means that the distribution function $F(E, L)$ is not uniquely determined by the mass density, and not even by the mass density together with the velocity dispersions.

The problem turns out no better when looking at one of the many possible forms of the inversion of (8) (Dejonghe 1986, hereafter Paper 2):

$$F'(E, L)=\frac{1}{\sqrt{\pi}}D_E^2\left[\sqrt{E}\int_0^1\frac{du}{\sqrt{1-u}}\int_0^{1-u}\frac{dv}{v\sqrt{1-v-u}}\varrho\left(Eu, \frac{L/\sqrt{2E}}{\sqrt{v}}\right)\right] \tag{9a}$$

and

$$F(E, L)=-\frac{1}{2^{3/2}\pi^{5/2}M}\,\mathrm{Im}\{F'(E, iL)\} \tag{9b}$$

with the remarkable property that we need $F'(E, t)$ in the purely imaginary argument $t=iL$, and subsequently should be able to take the imaginary part Im of that complex function. This is reminiscent of the inversion of the fundamental integral equation for axisymmetric systems in a form that was given first by Hunter (1975). It can be shown moreover that the type of inversion (9) is numerically unstable (Paper I). It is important to stress that this is a quite general

property of all inversion schemes. One is free to put forward some special forms for the distribution function, which parameterize solution space and are likely to lead to a simpler inversion. This has been done by a number of authors (Bouvier 1963; Veltmann 1965, and references therein; Kuz'min & Veltmann 1967; see also Fridman & Polyachenko 1984). However, the following formulae that relate the dispersions directly to the mass density are generally valid and convenient:

$$\sigma_r^2(\psi, r)=\frac{1}{\varrho(\psi, r)}\int_0^{\psi}\varrho(\psi', r)\,d\psi' \tag{10a}$$

$$\sigma_\varphi^2(\psi, r)=\sigma_\theta^2(\psi, r)=\frac{1}{\varrho(\psi, r)}\int_0^{\psi}D_{r^2}[r^2\varrho(\psi', r)]\,d\psi'. \tag{10b}$$

The expressions for the fourth moments are somewhat more elaborate:

$$\tau_{rr}^4(\psi, r)=\frac{1}{\varrho(\psi, r)}\int_0^{\psi}(\psi-\psi')\varrho(\psi', r)\,d\psi' \tag{11a}$$

$$\tau_{r\varphi}^4(\psi, r)=\tau_{r\theta}^4(\psi, r)=\frac{1}{3\varrho(\psi, r)}\int_0^{\psi}(\psi-\psi')D_{r^2}[r^2\varrho(\psi', r)]\,d\psi' \tag{11b}$$

$$\tau_{\varphi\varphi}^4(\psi, r)=\tau_{\theta\theta}^4(\psi, r)=3\tau_{\varphi\theta}^4(\psi, r)=\frac{1}{2\varrho(\psi, r)}\int_0^{\psi}(\psi-\psi')D_{r^2}^2[r^4\varrho(\psi', r)]\,d\psi'. \tag{11c}$$

It is important to know to what extent (9) can be useful. Though it is in principle hopeless to apply the inversion to the experimental determination of the distribution function, it remains to be seen whether in practice (e.g. taking into account that the distribution function should be positive) the formulae (9) really have the unstable character which essentially follows from purely mathematical considerations. We can proceed by constructing simple models and try to assess the freedom in distribution functions for fixed mass density $\varrho(r)$, fixed radial velocity dispersion profile $\sigma_r(r)$ and fixed tangential velocity dispersion profiles $\sigma_\varphi(r)=\sigma_\theta(r)$. This is the main purpose of Section 4, where we elaborate on a method for producing infinitely many distribution functions, all of which satisfy the above mentioned constraints.

3 The Plummer model

It will be clear from the foregoing section, that we definitely need a simple model in order to be able to calculate the distribution function analytically, which is – at least for our purpose here – necessary in order to avoid possible interference from the part of the numerically unstable inversion. Therefore, a Plummer (1911) model seems the most obvious candidate; the results obtained with this model are likely to be generic for a rather broad class of acceptable mass models without central singularity.

It is convenient to work with dimensionless quantities. We can fix the units by assigning a value to the gravitational constant G, the total mass M and to a distance unit r_s. Because the potential ψ enters the formulae so frequently, we will reserve a special symbol ψ_s for the unit of potential. We define

$$\psi_s=\frac{GM}{r_s}. \tag{12}$$

This unit of potential is a natural unit, as can be seen from the functional form for the potential at large radii. As a result, no unnecessary constants will appear when we express functions of the radius as functions of the (dimensionless) potential. Three of the four quantitites M, G, r_s and ψ_s

can be chosen arbitrarily. The remaining then follows from (12). We further choose $\psi(0)=1$, so that ψ_s is the value of the potential at the centre of the spherical system, and therefore (12) is a genuine constraint on the units.

In these units, the Plummer model is defined by the potential

$$\psi(r)=\frac{1}{\sqrt{1+r^2}}, \tag{13}$$

with the corresponding mass density

$$\varrho(r)=\frac{3}{4\pi}(1+r^2)^{-5/2}. \tag{14}$$

By combination of (13) and (14) we may write $\varrho=\varrho(\psi)$, with

$$\varrho(\psi)=\frac{3}{4\pi}\psi^5. \tag{15}$$

In the isotropic case, the distribution function follows immediately from (4):

$$F(E)=\frac{3}{7\pi^3}(2E)^{7/2}, \tag{16}$$

with a velocity dispersion profile

$$\sigma^2(r)=\frac{1}{6}\frac{1}{\sqrt{1+r^2}}. \tag{17}$$

3.1 THE ANISOTROPIC MODEL

We have seen in Section 2 that anisotropic models can be constructed by expression of ϱ as a function of both ψ and r. The simple form of $\psi(r)$ suggests the following choice for the function $\varrho(\psi, r)$

$$\varrho_q(\psi, r)=\frac{3}{4\pi}\psi^{5-q}(1+r^2)^{-q/2}, \tag{18}$$

with one parameter q, but leading for all q to the same mass density (14). The distribution function $F_q(E, L)$ that is consistent with $\varrho_q(\psi, r)$ now follows from (9). Details of the calculation can be found in Paper I:

$$F_q(E,L)=\frac{3\Gamma(6-q)}{2(2\pi)^{5/2}\Gamma(\tfrac{1}{2}q)}E^{7/2-q}\,\mathbb{H}\left(0, \tfrac{1}{2}q, \tfrac{5}{2}-q, 1; \frac{L^2}{2E}\right), \tag{19}$$

where $\Gamma(x)$ denotes the gamma function. The function $\mathbb{H}(a, b, c, d; x)$ is defined by means of its Mellin transform (see appendix A2 of Paper I). For computational purposes it can be expressed conveniently in terms of the hypergeometric function:

$$\mathbb{H}(a, b, c, d; x)=\begin{cases}\dfrac{\Gamma(a+b)}{\Gamma(c-a)\Gamma(a+d)}x^a\,{}_2F_1(a+b, 1+a-c; a+d; x), & x\le 1;\\[2ex] \dfrac{\Gamma(a+b)}{\Gamma(d-b)\Gamma(b+c)}\left(\dfrac{1}{x}\right)^b{}_2F_1\left(a+b, 1+b-d; b+c; \dfrac{1}{x}\right), & x\ge 1.\end{cases} \tag{20}$$

We refer to Section 4 for some plots of distribution functions. Positiveness of $F_q(E, L)$ restricts the possible parameter values to $q \leqslant 2$. When $q<2$, the distribution functions are non-negative over the full region in phase space which is in principle accessible, and are zero only for $E=0$. This is an interesting property in view of stability requirements. The limiting case $q=2$ gives rise to a very simple distribution function (see Osipkov 1979). It is also identical to one of the Merritt (1985) models (with anisotropy parameter $r_a=1$):

$$F_2(E, L)=\begin{cases} \dfrac{6}{(2\pi)^3}(2E-L^2)^{3/2}, & L^2 \leqslant 2E; \\ 0, & L^2 \geqslant 2E. \end{cases} \tag{21}$$

Their special character also follows from (18), which shows the simple form of those models when expressed as a function of ψ and r; to reproduce the models considered by Merritt however, r should be replaced by r/r_a. The distribution function is zero in a subset of the accessible phase space. However, perturbations applied on systems with this kind of distribution functions will tend to fill up this space, and it is unlikely that the system ever will return to the initial condition (21).

The quantity q will appear as a parameter in every model from now on. It therefore serves no purpose to carry the index q throughout the formulae. We will systematically omit it in this section in order to avoid cumbersome notations.

3.2 SOME LOWER-ORDER MOMENTS

Physical understanding of q is provided by the expressions for the velocity dispersions. By means of equations (10) we obtain

$$\sigma_r^2(r)=\frac{1}{6-q}\frac{1}{\sqrt{1+r^2}} \tag{22a}$$

and

$$\sigma_\varphi^2(r)=\sigma_\theta^2(r)=\frac{1}{6-q}\frac{1}{\sqrt{1+r^2}}\left(1-\frac{q}{2}\frac{r^2}{1+r^2}\right). \tag{22b}$$

Whence, Binney's anisotropy parameter β equals the monotonic function

$$\beta=1-\frac{\sigma_\varphi^2}{\sigma_r^2}=1-\frac{\sigma_\theta^2}{\sigma_r^2}=\frac{q}{2}\frac{r^2}{1+r^2}. \tag{23}$$

This means that q has the same sign as β. It follows from the definition of β that the near-radial orbits are prevalent if $\beta>0$, and conversely that the near-circular orbits are favoured in a $\beta<0$ cluster. We will call the latter tangential orbits. When $\beta=0$, both types are balanced in the isotropic sense. The anisotropy parameter equals zero at $r=0$ regardless of the value of q. However, the value of the dispersions at the centre changes with q. When q becomes very negative, we see from (22a) that $\sigma_r^2(r)$ approaches zero. This means that in the limit $q \to -\infty$ the cluster contains only circular orbits. The other limiting case, $q=2$, has an anisotropy parameter β that tends to 1 for large radii, which means that in the outer parts only radial orbits are present. We will henceforth denote clusters according to the prevalent type of orbits at large radii. In this family and with this convention, radial clusters have $0<q<2$; tangential clusters have $q<0$ and the isotropic cluster has $q=0$.

The fourth moments are of special importance in the sequel. Using (11) we find easily

$$\tau^4_{rr}(\psi, r)=\frac{9}{4\pi}\,\frac{1}{(7-q)(6-q)}\,\frac{1}{1+r^2}, \tag{24a}$$

$$\tau^4_{r\varphi}(\psi, r)=\tau^4_{r\theta}(\psi, r)$$

$$=\frac{3}{4\pi}\,\frac{1}{(7-q)(6-q)}\,\frac{1}{1+r^2}\left(1-\frac{q}{2}+\frac{q}{2}\,\frac{1}{1+r^2}\right), \tag{24b}$$

$$\tau^4_{\varphi\varphi}(\psi, r)=\tau^4_{\theta\theta}(\psi, r)=3\tau^4_{\varphi\theta}(\psi, r)$$

$$=\frac{9}{8\pi}\,\frac{1}{(7-q)(6-q)}\,\frac{1}{1+r^2}$$

$$\times\left[\left(2-\frac{q}{2}\right)\left(1-\frac{q}{2}\right)-2\left(1-\frac{q}{2}\right)\left(-\frac{q}{2}\right)\frac{1}{1+r^2}+\frac{q}{2}\left(\frac{q}{2}+1\right)\frac{1}{(1+r^2)^2}\right]. \tag{24c}$$

Higher-order moments are rather abstract but can be important technically (see the calculation of the line profiles). Their definition and a general expression can be found in Appendix A and Paper I.

3.3 THE ENERGY DISTRIBUTION

It is important to investigate the influence of anisotropy on the energy distribution of the stars at a certain radius r. This distribution is the marginal distribution of $F(E, L)$ after integration with respect to v_T. Following (8), we have

$$F_E(\psi, r, E)=2\pi\int_0^{2(\psi-E)}\frac{F(E, L)}{\sqrt{2(\psi-E)-v_T^2}}\,dv_T^2. \tag{25}$$

For this family, the integral (25) can be calculated explicitly (Paper I). The result is

$$F_E(\psi, r, E)=\frac{3}{4\pi}\,\frac{\Gamma(6-q)}{\Gamma(\tfrac{1}{2}q)}\,\frac{E^{4-q}}{r}\,\mathbb{H}\left(\tfrac{1}{2}, \tfrac{1}{2}(q-1), 5-q, 1; r^2\frac{\psi-E}{E}\right), \tag{26}$$

again easily expressible through (20) in terms of the hypergeometric function. In the isotropic case, we of course recover

$$F_E(\psi, r, E)=4\pi F(E)\sqrt{2(\psi-E)}. \tag{27}$$

Fig. 1 shows these marginal distributions $F_E(\psi(r), r, E)$, both in the centre and at a fairly large radius. The abscissae are normalized to $\psi(r)$. We know that in a radial cluster, orbits are more radial in the outer parts. Therefore, the stars must be around their turning points: their orbits cannot extend much farther, because the mass density falls off rather steeply. This means that they are relatively strongly bound, which is evident in the figure. This argument, however, is not applicable for tangential clusters because the effect of turning points is much less, as the stars are moving in rather circular orbits. At a small radius, the situation is reversed. If we had maintained the same energy structure for a radial cluster as at the edge, the centre would have become overpopulated (the mass density is kept fixed). As a result, the energy peak moves to the left. Equivalently, since a tangential cluster contains nearly circular orbits at the edge, the same energy structure would produce a hole in the core. We thus need to fill it up with radial orbits. This feature is generally true for these models and could be called the complementarity property:

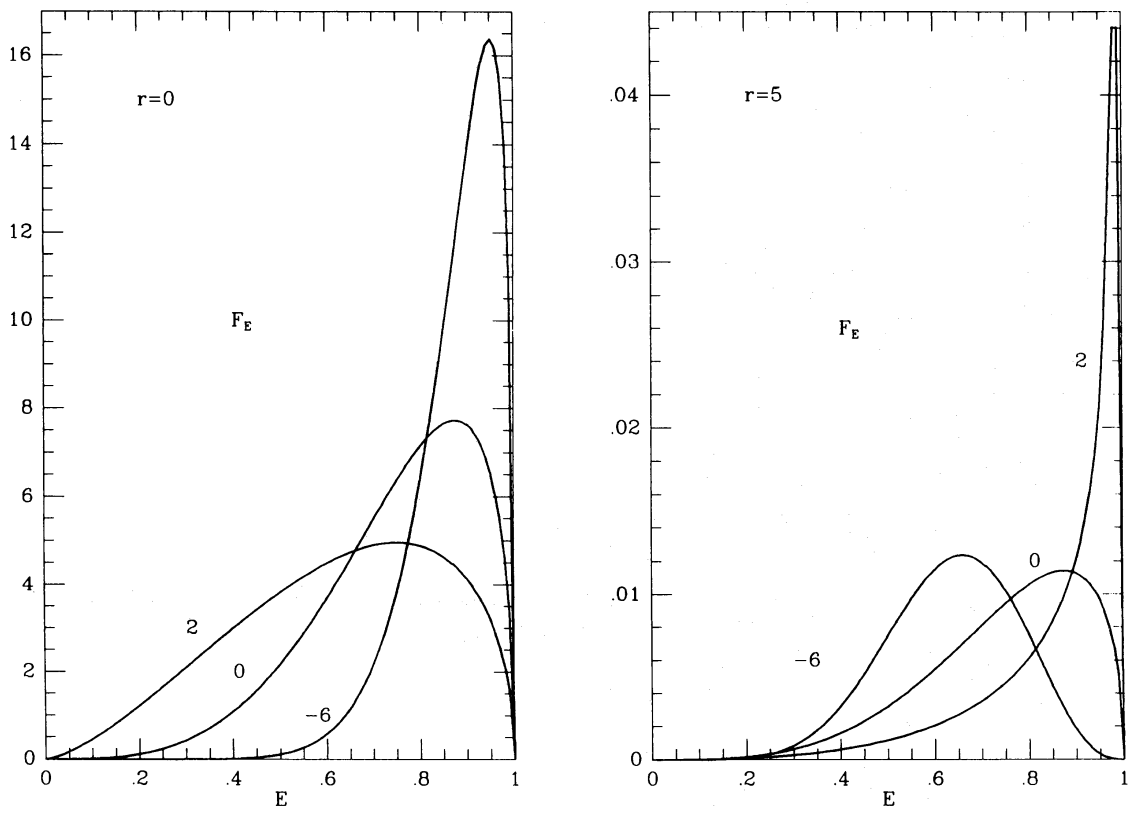

Figure 1. Distribution of the binding energies (irrespective of angular momentum) at spatial radii $r=0$ and $r=5$. Values of q are indicated. The energy is normalized with respect to the maximum binding energy at a given radius $\psi(r)$. The total area under each curve is proportional to the local mass density.

if a more radial cluster dominates a more tangential one in a specified dynamical variable in the centre, then the more tangential one will dominate the more radial in that same dynamical variable at the edge, and vice versa; moreover, the transition radius is usually close to the core radius. The explicit form for the distribution of the binding energy at radius r, given by (26), enables us to calculate the mean value of the energy at each radius. We find

$$\mu_E(r)=\frac{3}{8\pi}\frac{1}{(6-q)}\frac{1}{(1+r^2)^3}\left(9-q-q\frac{1}{1+r^2}\right). \tag{28}$$

Fig. 2 shows the mean energy profile as a function of spherical radius r, normalized with respect to the isotropic mean energy curve. The conclusions that could already be drawn from Fig. 1 are now apparent. The curves have the same peculiarity as the projected dispersion profiles: they all pass through one point at $r=1$, of course for the same reason. We find $\mu_E(1)=9/(2^7\pi)$.

Another interesting function gives the probability of finding a particle with binding energy E, irrespective of position. It is defined as

$$N(E)=2\pi\int_0^{r(E)} F_E(\psi,r,E)\,r^2\,dr, \tag{29}$$

with $r(E)$ the largest distance at which a binding energy E can occur. The single integration is not worth the analytical effort; the function $N(E)$ is calculated numerically. Fig. 3 shows some curves for different values of q. By and large, they don't differ very drastically. A variation of the orbital structure apparently is not effective in changing the population of the energy surfaces, at least in the cases considered.

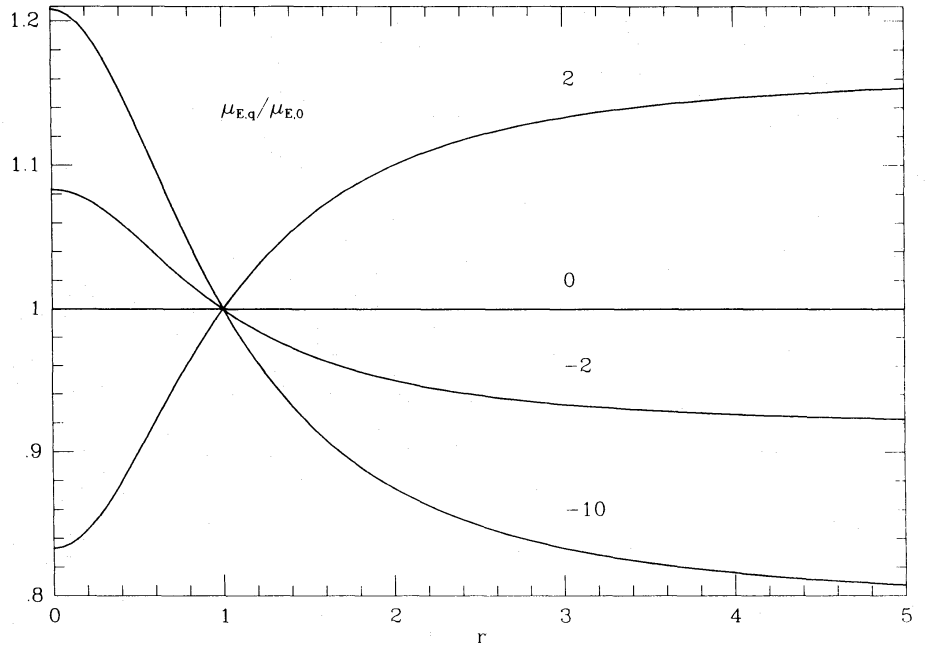

Figure 2. The mean energy as a function of spherical radius, normalized to the mean energy of the isotropic case. Values of q are indicated.

The discussion of the energy structure of the cluster is complete with the calculation of the total energy. We easily find

$$E_{\rm tot}=4\pi\int_0^{+\infty}[\mu_{\rm E}(r)-\tfrac{1}{2}\psi(r)\varrho(r)]r^2\,dr$$

$$=\frac{3\pi}{2^6}. \tag{30}$$

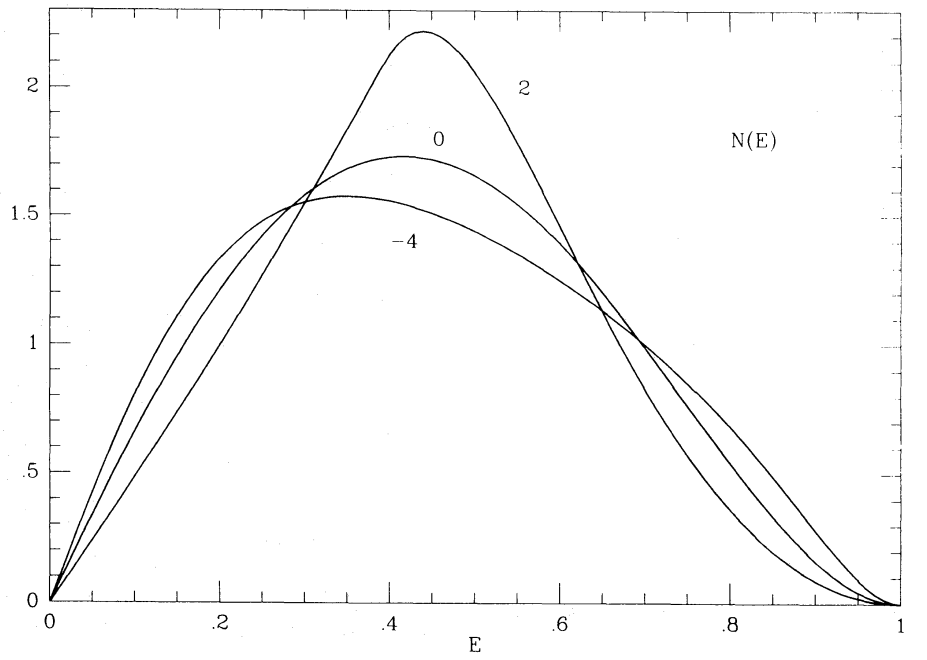

Figure 3. The binding energy probability function $N(E)$. The values of q are indicated.

The total energy is thus constant for all the models: the excess in binding energy that tangential clusters show in the central parts is thus exactly compensated for at the outer parts. This can easily be explained with the virial theorem. We know, due to virial equilibrium, that

$$E_{\rm tot}=V_{\rm tot}-T_{\rm tot}=\tfrac{1}{2}V_{\rm tot}=T_{\rm tot}, \tag{31}$$

with $T_{\rm tot}$ the total kinetic energy and $V_{\rm tot}$ the total (positive) potential energy. Because the right-hand side of (31) does not involve any quantity other than the mass density and the potential, which are the same for all our models, the total binding energy must be the same too.

3.4 THE DISTRIBUTION OF THE TRANSVERSE MOTIONS

We can now go through the same exercise as we did for the energies, in order to calculate the distribution of the transverse velocity $v_{\rm T}$ at radius r. This distribution is given by the integral

$$F_{v_{\rm T}}(\psi, r, v_{\rm T})=2^{3/2}\pi v_{\rm T}\int_0^{\psi-v_{\rm T}^2/2}\frac{F(E, L)\,dE}{\sqrt{\psi-E-\tfrac{1}{2}v_{\rm T}^2}} \tag{32}$$

which is found to be (Paper I)

$$F_{v_{\rm T}}(\psi, r, v_{\rm T})=\frac{3}{2^{6-q}\pi}\frac{\Gamma(6-q)}{\Gamma(\tfrac{1}{2}q)}\frac{L^{9-2q}}{r}\mathbb{H}\left(4-\tfrac{1}{2}q, q-4, 5-q, 1; \frac{2\psi-v_{\rm T}^2}{L^2}\right). \tag{33}$$

Fig. 4 shows some representative examples for a central location and for a large radius. The abscissae are normalized with respect to the escape velocity $\sqrt{2\psi}$. Especially at large radii we find

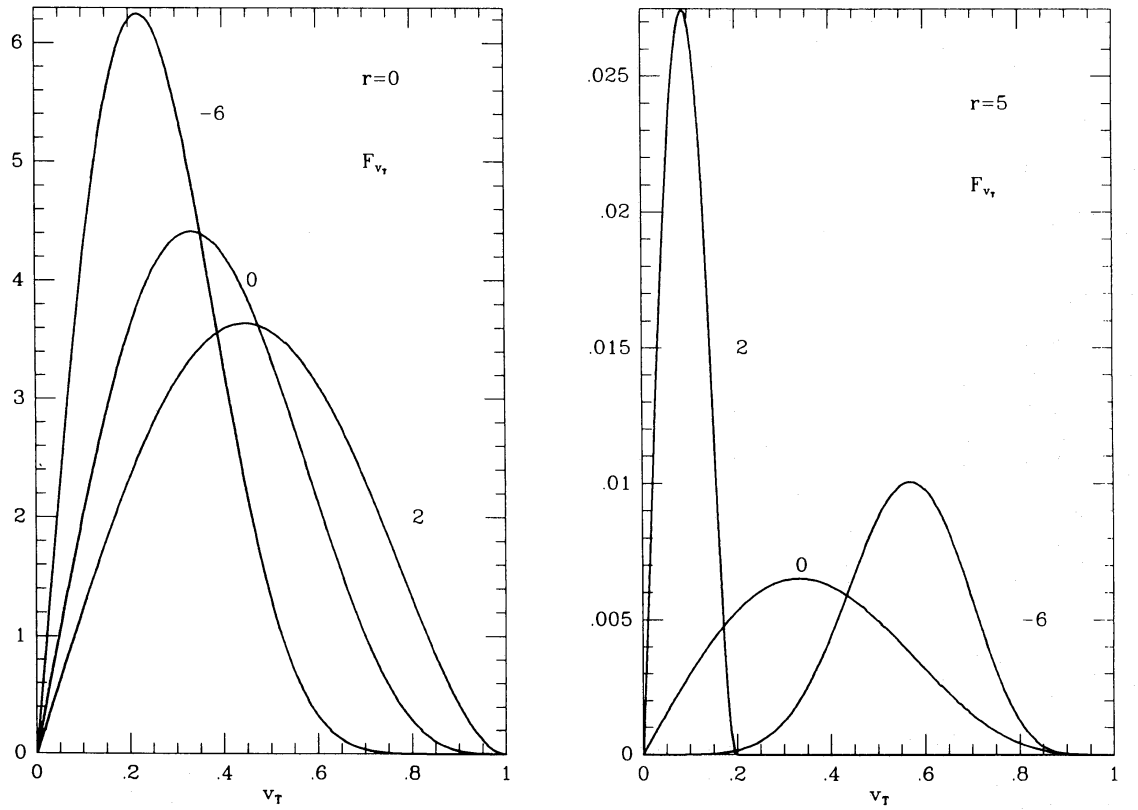

Figure 4. Some distributions of the transverse velocities (irrespective of energy) at spatial radii $r=0$ and $r=5$. Values of q are indicated. The transverse velocity is normalized so that the maximum velocity at a given radius equals one. The total area under each curve is proportional to the local mass density.

most stars at their turning points in radial clusters, while the effect of the turning points in a tangential cluster is not so important by the very nature of the prevalent type of orbits there, which are more circular.

We now calculate the mean of the square of the transverse velocity v_T^2. This is a measure of the kinetic energy in transverse motion at spherical radius r. We find

$$\mu_{v_T^2/2}(r)=\frac{3}{8\pi}\frac{1}{6-q}\frac{1}{(1+r^2)^3}\left(2-q\frac{r^2}{1+r^2}\right). \tag{34}$$

Fig. 5 shows some transverse energy profiles. The different character of tangential and radial clusters at small and large radii is again apparent. At the centre, radial clusters have more energy in transverse motion than tangential clusters. The opposite is true in the outer parts. The fixed point occurs now for $r=\sqrt{1/2}$ and equals $1/(27\pi)$. Finally, an elementary integration allows us to calculate the total kinetic energy in transverse motion T_T of the cluster. We find (using 30)

$$T_T=E_{tot}\left(1-\frac{2}{6-q}\right). \tag{35}$$

This is a monotonically decreasing function of q, which was to be expected. We further remark that when $q=0$, two thirds of the kinetic energy is locked in the transverse motions, in virtue of (31) and (35), confirming a well-known feature of isotropic models.

3.5 SOME PROJECTED MOMENTS

We can associate with every spherical quantity $f(r)$ its projection $f_p(r_p)$ on the plane of the sky. The radius r_p is the projected radius in the plane. Elementary geometry shows that

$$f_p(r_p)=2\int_{r_p}^{+\infty}\frac{r\,dr}{\sqrt{r^2-r_p^2}}f(r). \tag{36}$$

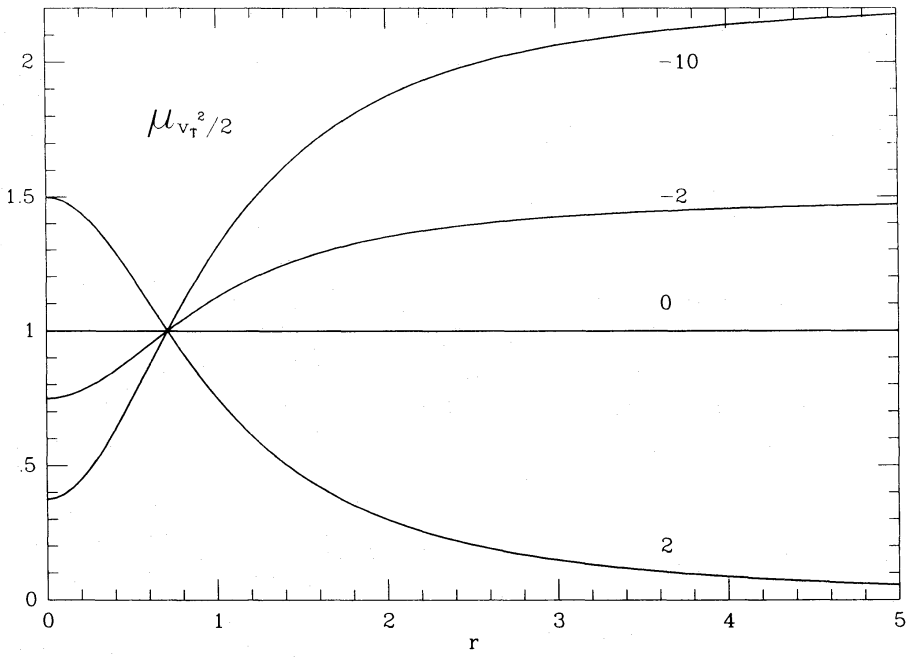

Figure 5. The mean energy in transverse motions as a function of spherical radius, normalized to the mean transverse kinetic energy of the isotropic case. Values of q are indicated.

We find for the projected mass density $\varrho_p(r_p)$:

$$\varrho_p(r_p)=2\int_{r_p}^{+\infty}\frac{r\,dr}{\sqrt{r^2-r_p^2}}\varrho(r)=\frac{1}{\pi}\frac{1}{(1+r_p^2)^2}. \tag{37}$$

Whence, if we define the core radius as the radius at which $\varrho_p(r_p)$ drops to half of its central value, we find

$$r_c=\sqrt{\sqrt{2}-1}\simeq 0.64. \tag{38}$$

The cumulative mass function $M_p(r_p)$ equals

$$M_p(r_p)=2\pi\int_0^{r_p}\varrho_p(r_p')\,r_p'\,dr_p'=\frac{r_p^2}{1+r_p^2} \tag{39}$$

and therefore $r_p=1$ is the radius of the cylinder that contains half of the total mass.

The projected velocity dispersion profile $\sigma_p(r_p)$ as a function of the projected radius r_p monotonically decreases in radial and isotropic clusters, but it can have a maximum in tangential clusters, because the tangential component of the velocity dispersion becomes increasingly important when observing more at the edge of the cluster. This effect can be readily calculated in the case of this anisotropic Plummer model. The projected spatial velocity v_p along the line-of-sight is given by

$$v_p=\frac{z}{r}v_r+\frac{r_p}{r}v_\varphi, \tag{40}$$

with

$$r^2=z^2+r_p^2, \tag{41}$$

because we can always rotate the v_θ and v_φ axes – in virtue of the isotropy in v_θ and v_φ – so that the v_θ axis is orthogonal to the line-of-sight. The projected velocity dispersion $\sigma_p(r_p)$ is therefore generally given by [see also Binney & Mamon (1982)]

$$\sigma_p^2(r_p)\varrho_p(r_p)=2\int_{r_p}^{+\infty}\frac{r\,dr}{\sqrt{r^2-r_p^2}}\varrho(r)\left\{\sigma_r^2(r)\left[1-\frac{r_p^2}{r^2}\beta(r)\right]\right\}. \tag{42}$$

With this equation, (22a), (23) and (37) we find

$$\sigma_p^2(r_p)=\frac{3\pi}{32}\frac{1}{6-q}\frac{1}{\sqrt{1+r_p^2}}\left(3-\frac{5q}{4}\frac{r_p^2}{1+r_p^2}\right). \tag{43}$$

Fig. 6 shows some representative examples. For $q\leqslant -6/5$, there is a maximum in $\sigma_p^2(r_p)$ at $r_p^2=-2(5q+6)/(12-5q)$. Furthermore, all profiles $\sigma_p^2(r_p)$ pass through the same point $\sigma_p^2=3\pi\sqrt{3/5}/64$ at $r_p=\sqrt{2/3}$. This is to be considered as a peculiarity of this particular family, though a quite general feature in these models. It is a consequence of the fact that the parameter q enters linearly in both numerator and denominator.

Finally, even in the projected velocity dispersions we clearly recognize the complementarity property. The projected velocity dispersion of a radial cluster dominates the projected velocity dispersion of a tangential cluster in the centre, but a tangential cluster dominates a radial one at the edge. The transition radius is close to the core radius. The information contained in equations (22) is reflected in the figure. Anisotropic clusters show their true character at large radii. Radial clusters have less projected velocity dispersion at large r_p because the radial motions don't contribute significantly to the line-of-sight motions.

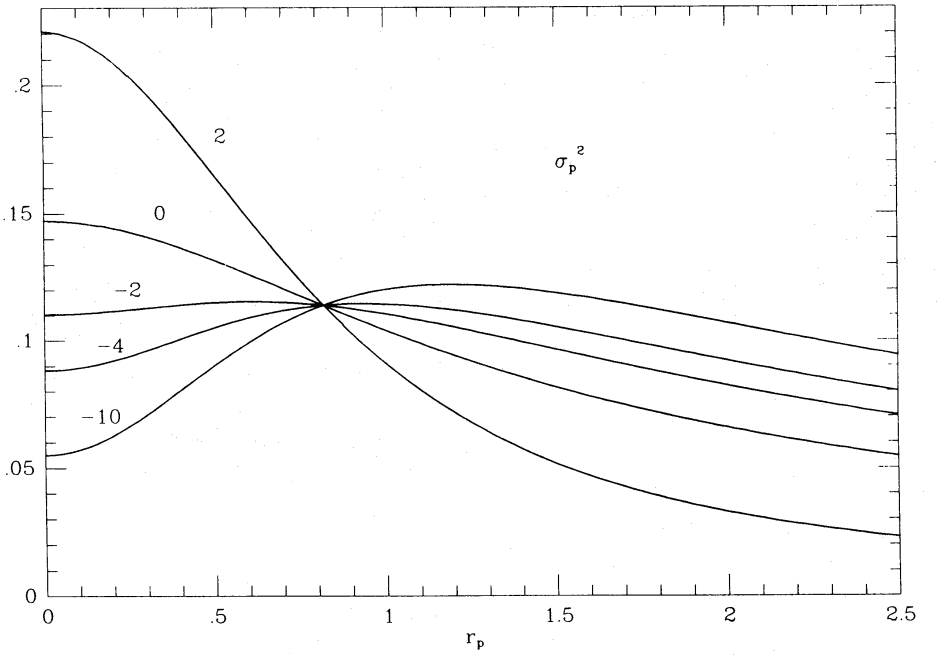

Figure 6. The projected velocity dispersion as function of projected radius. Values of q are indicated. For an explanation of the fixed point: see text.

The calculation of the fourth moment $\tau_p^4(r_p)$ of the projected velocity distribution is not fundamentally different from the above derivation of $\sigma_p^2(r_p)$, but more elaborate. We find

$$r_p^4(r_p)=\frac{12}{5}\frac{1}{(7-q)(6-q)}\frac{1}{1+r_p^2}\left[1-\frac{6q}{7}\frac{r_p^2}{1+r_p^2}+\frac{2}{21}q(q+2)\frac{r_p^4}{(1+r_p^2)^2}\right]. \tag{44}$$

Instead of the fourth moment, one preferably considers the dimensionless kurtosis $kur=\tau_p^4/\sigma_p^4$

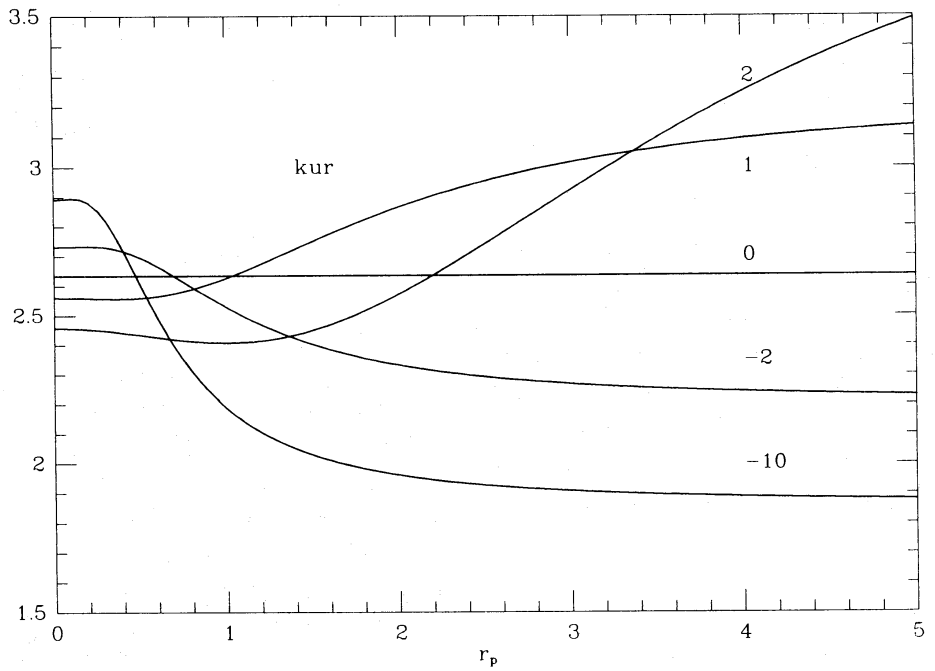

Figure 7. The kurtosis of the line-of-sight velocity distribution (line profile) as a function of projected radius. Values of q are indicated.

to measure the degree to which the distribution is peaked. The smaller the kurtosis, the more peaked the distribution. A Gaussian distribution has $kur=3$. Fig. 7 shows some kurtosis profiles for various models. Of course, those curves are not so markedly different as is the case for the dispersion profiles. This stems primarily from the fact that the higher-order moments are more and more dominated by the tails of the distribution, and the projected velocity distribution has vanishing tails anyway (due to the cut-off at the escape velocity). Only radial models show, despite the finite tails, a kurtosis which is greater than 'normal': they are too bulky around escape velocity. This is a consequence of the relatively small exponent of the energy factor in the expression for the distribution function (19).

3.6 THE LINE PROFILES

As a final step in the exploration of the model, we calculate the observable radial velocity line profiles. A line profile $\mathrm{lp}_{r_p}(v_p)$ at a particular projected radius r_p is defined as the distribution of the velocities v_p projected along the line of sight (and which are therefore the observed radial velocities). In order to calculate them, we need for every projected radius r_p and every projected velocity v_p to perform a triple integration: two of them integrate over three-dimensional velocity space, reducing its dimensionality to one, and the last integrates through the cluster along the line-of-sight. This is a somewhat tricky calculation, and it is worthwhile to try to avoid it. Within the assumption of a Gaussian velocity distribution, some line profiles were calculated by Tonry (1983). Unfortunately, we cannot make this assumption here. Instead of doing the triple numerical integration, it is possible to devise a short cut which enables us to calculate the line profile within a better accuracy than the probable observational errors. It is convenient to work with velocities v that are normalized with respect to the greatest possible projected radial velocity v_p we can observe at a particular r_p. This velocity equals $\sqrt{2\psi(r_p)}$, with $\psi(r)$ the Plummer potential (13). We therefore take

$$v=\frac{v_p}{\sqrt{2\psi(r_p)}}. \tag{45}$$

We moreover normalize the total area under the line profile to one, though it is actually proportional to the projected mass density (37).

We now use the expansion

$$\mathrm{lp}_{r_p}(v)\,dv=(1-v^2)^{5-\alpha}\left[c_0+\sum_{i\geq 1}c_i(1-v^2)^i\right]dv. \tag{46}$$

The first term is calculated in Appendix C (α varies according to whether one is looking at the core or at the edge) and is essentially the asymptotical form of the tails of lp_{r_p}. The additional terms in c_i, $i\geq 1$ are correction terms: the coefficients c_i can be determined by the known moments of the distribution. The zeroth moment of course should be one, the second and the fourth are proportional to (43) and (44), respectively. Here again we see the great advantage of having at our disposal an analytical form for $\varrho(\psi, r)$, as given by (18). Better still, in this case all higher order moments of $\mathrm{lp}_{r_p}(v)$ can be calculated analytically with formulae analogous to (10) and (11) and integrations analogous to (42). We already see from (43) and (44) that the full $2n$th order moment will be given by a factor $(1+r_p^2)^{-n/2}$ multiplied by a nth order polynomial in $r_p^2/(1+r_p^2)$. They are calculated systematically in Appendix A. The general expression for the moments of the renormalized distibution, which were actually used in the computations, is given by

$$\mu^{2n}=\tfrac{3}{4}\Gamma(6-q)\,\frac{\Gamma(n+\tfrac{1}{2})}{\Gamma(n+6-q)}\,\frac{\Gamma(\tfrac{1}{2}n+2)}{\Gamma(\tfrac{1}{2}n+\tfrac{5}{2})}\,{}_3F_2\left(-n,\ \tfrac{1}{2}q,\ \tfrac{1}{2}n+2;\ 1,\ \tfrac{1}{2}n+\tfrac{5}{2};\ \frac{r_p^2}{1+r_p^2}\right). \tag{47}$$

These higher order moments ($n \geq 3$) will add to the accuracy of the approximation (46). The calculations here were done with six moments and with the additional condition that $\mathrm{lp}_{r_p}(0)$ equals the exact value (see Appendix B):

$$\mathrm{lp}_{r_p}(0) = \frac{3}{4}\frac{\Gamma(6-q)\,\Gamma(7/4)}{\Gamma(11/2-q)\,\Gamma(9/4)}\,{}_3F_2\left(1/2,\ 1/2q,\ 7/4;\ 1,\ 9/4;\ \frac{r_p^2}{1+r_p^2}\right). \tag{48}$$

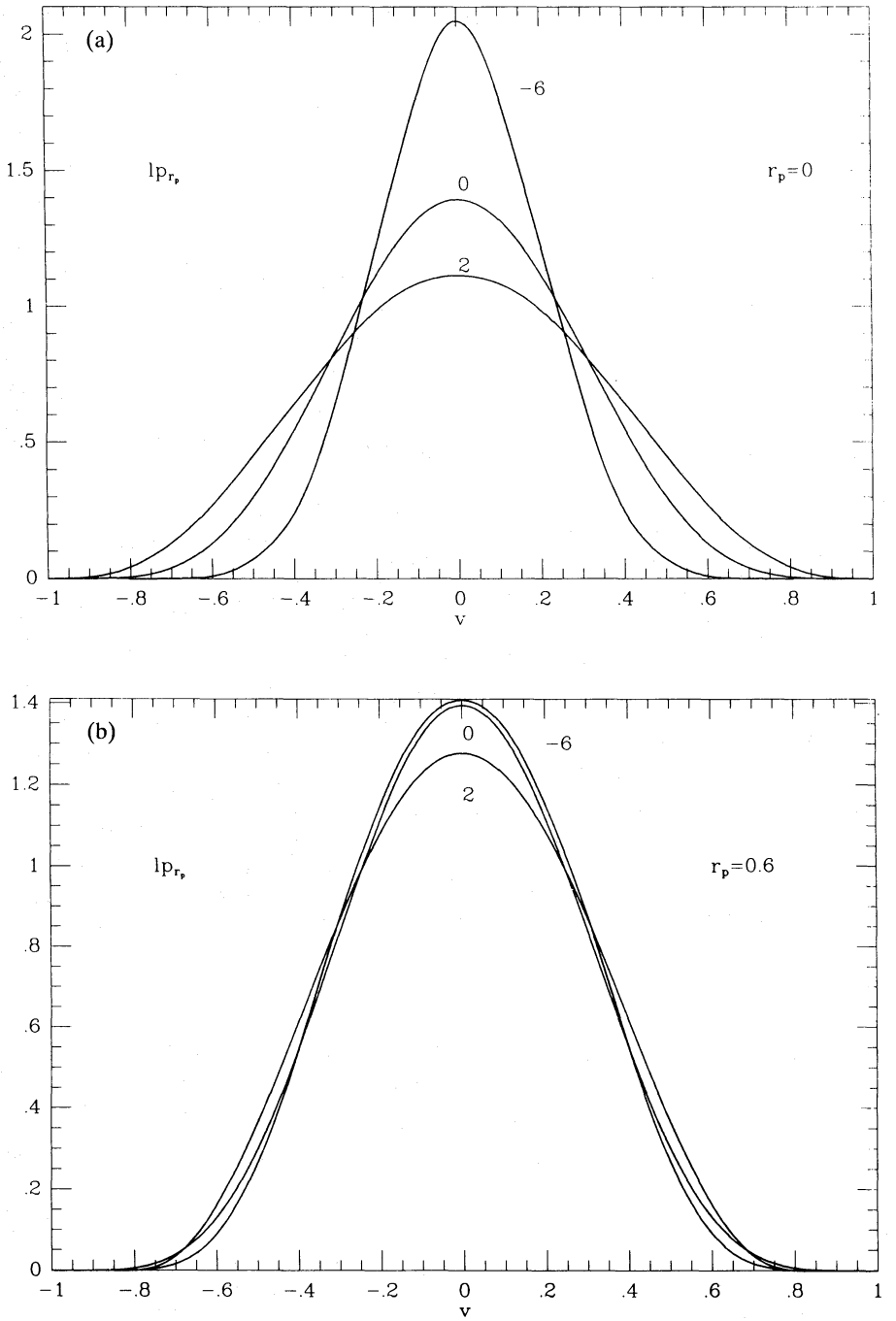

Figure 8. (a) Some typical line profiles along the line-of-sight through the centre. Values of q are indicated. Velocities are normalized, as is the total area under the profiles. (b) Some typical line profiles at core radius. Values of q are indicated. Velocies are normalized, as is the total area under the profiles. (c) Some typical line profiles at the edge. Values of q are indicated. Velocities are normalized as is the total area under the profiles.

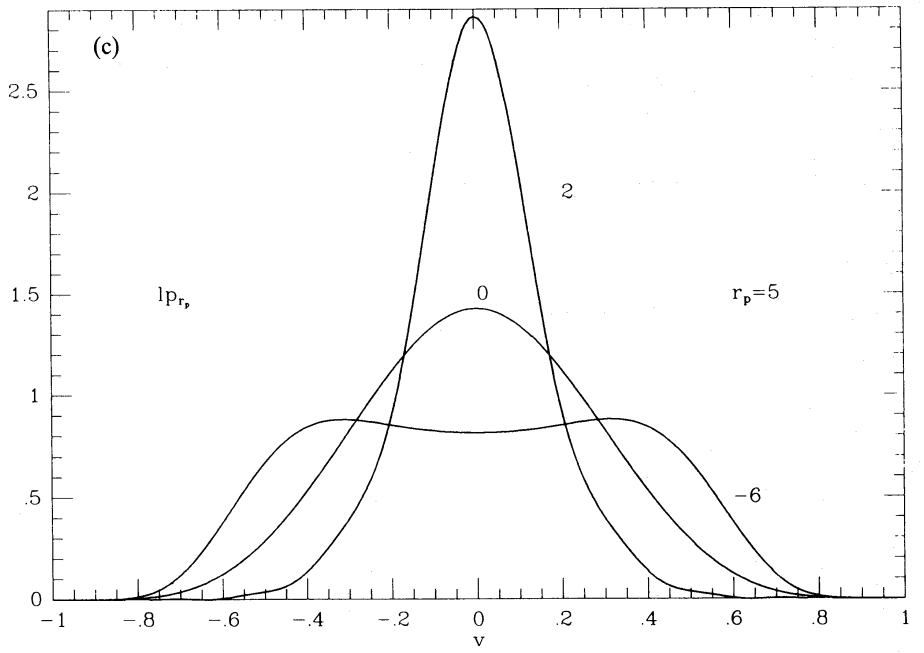

Figure 8 – *continued*

This procedure is superior to the brute force integration, which has been performed as a check at some points.

Fig. 8(a) shows some typical lines at the centre. The ordinate is the normalized velocity v and the total area under the curve, which is actually equal to the projected mass density (37), is normalized to one. The most striking feature is a confirmation of Fig. 6: tangential clusters have a more peaked projected velocity distribution. Fig. 8(b) features the same lines but now at the core radius. The different types are virtually indistinguishable there. At large radius, Fig. 8(c), we see even a qualitative difference. Tangential clusters show bimodal lines, arising from the nearly circular orbits, with stars populating them in both senses in equal amount (no net streaming). Radial clusters persist in the old unimodal type of profile. Again, as a consequence of the complementarity property, the conclusions to be drawn from the line profiles depend essentially on the region one is looking at, e.g. line profiles for globular clusters which are the result of star counts in the outer parts should be interpreted with the aid of Fig. 8(c). On the other hand, Fig. 8(a) applies to line profiles that are measured in the core of a giant elliptical.

4 More distribution functions

As was already pointed out in the introduction, the indeterminacy in $F(E, L)$ comes essentially from the degeneracy $\varrho(\psi, r) \equiv \varrho(r)$. It is only natural to exploit this factor to construct distribution functions that all give rise to the same spatial mass density $\varrho(r)$ and the same spatial velocity dispersions $\sigma_r^2(r)$, $\sigma_\varphi^2(r) = \sigma_\theta^2(r)$. It suffices to notice that

$$\gamma(\psi, r) = \psi^2(r^2+1) \tag{49}$$

effectively equals one when expressed as a function of r. Let now σ_r^2 be written as some function of the three arguments ψ, r and γ. Then we have as a consequence of (10):

$$\varrho(\psi, r) = D_\psi[\varrho\sigma_r^2(\psi, r)], \tag{50a}$$

$$\varrho\sigma_\varphi^2(\psi, r) = \varrho\sigma_\theta^2(\psi, r) = D_{r^2}[r^2\varrho\sigma_r^2(\psi, r)]. \tag{50b}$$

Rewriting them as functions of the three variables ψ, r and γ:

$$\varrho(\psi,r,\gamma)=D_\psi[\varrho\sigma_r^2(\psi,r,\gamma)]+D_\gamma[\varrho\sigma_r^2(\psi,r,\gamma)]\,D_\psi\gamma(\psi,r), \tag{51a}$$

and

$$\varrho\sigma_\varphi^2(\psi,r,\gamma)=\varrho\sigma_\theta^2(\psi,r,\gamma)=\varrho\sigma_r^2(\psi,r,\gamma)$$
$$+r^2D_{r^2}[\varrho\sigma_r^2(\psi,r,\gamma)]+r^2D_\gamma[\varrho\sigma_r^2(\psi,r,\gamma)]\,D_{r^2}\gamma(\psi,r). \tag{51b}$$

A sufficient condition that $\varrho(\psi(r),r,1)$ and $\sigma_\varphi^2(\psi(r),r,1)=\sigma_\theta^2(\psi(r),r,1)$ remains unchanged therefore is

$$D_\gamma[\varrho\sigma_r^2(\psi,r,\gamma)]|_{\gamma=1}=0, \tag{52}$$

for all $\sigma_r^2(\psi(r),r,1)$ that are compatible with the data.

As an application, we generalize (10a) and (17) by

$$\varrho\sigma_r^2(\psi,r,\gamma)=\frac{3}{4\pi}\frac{1}{6-q}\psi^{6-q}(1+r^2)^{-q/2}[1+a(1-\gamma)^n], \qquad \text{with} \quad n\geq 2. \tag{53}$$

Many more generalizations are of course possible. Applying now (50a), we find

$$\varrho_{q,n,a}(\psi,r,\gamma)=\frac{3}{4\pi}\psi^{5-q}(1+r^2)^{-q/2}[1+a(1-\gamma)^n-\frac{2na}{6-q}\gamma(1-\gamma)^{n-1}]. \tag{54}$$

The parameter space has thus been extended with the discrete parameter n and a continuous parameter a. For fixed q, (54) is the expression of a two-parameter family of models, all with the same mass density and spatial velocity dispersions. Expanding (54) in powers of γ, we find

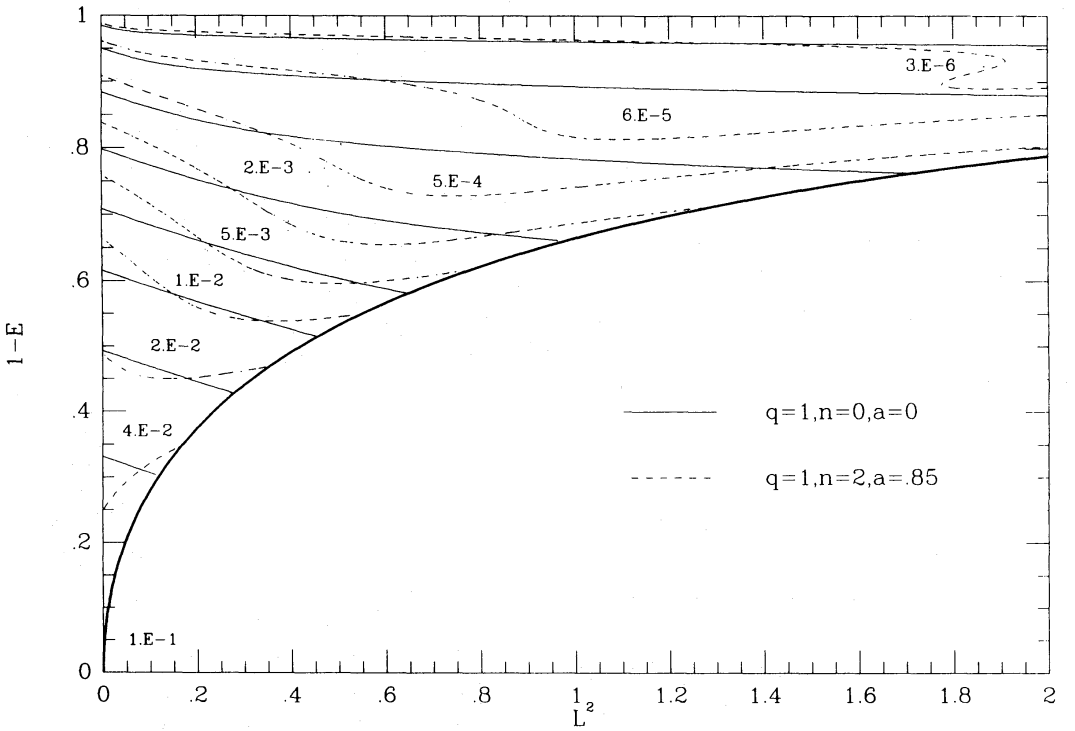

Figure 9. Two distribution functions compatible with a $q=1$ radial model. The heavy curve is the locus of the circular orbits. The isoprobability contours are plotted for both surfaces. The values of the distribution functions along the contours is indicated.

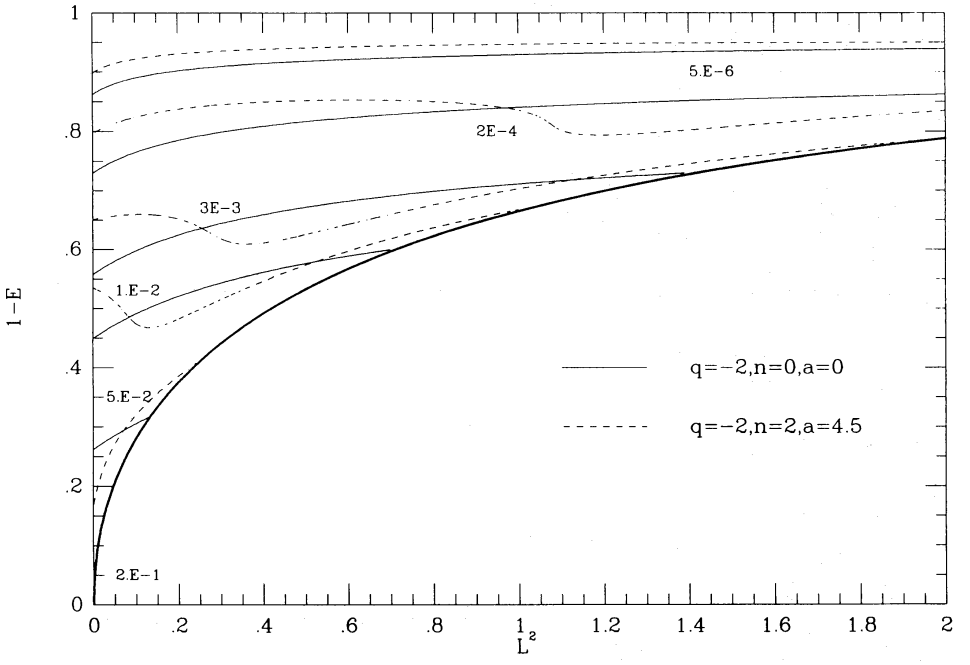

Figure 10. Same as Fig. 9, but for two $q=-2$ tangential models.

after some algebra

$$\varrho_{q,n,a}(\psi, r)=(1+a)\varrho_q+a\sum_{i=1}^{n}(-1)^i\left[\binom{n}{i}+\frac{2n}{6-q}\binom{n-1}{i-1}\right]\varrho_{q-2i}. \tag{55}$$

This is a particularly useful formula, because the same relationship applies to all quantities which are linear in ϱ, e.g. (55) can be used to determine distribution functions; we only have to replace ϱ by F:

$$F_{q,n,a}(\psi, r)=(1+a)F_q+a\sum_{i=1}^{n}(-1)^i\left[\binom{n}{i}+\frac{2n}{6-q}\binom{n-1}{i-1}\right]F_{q-2i}. \tag{56}$$

Figs 9 and 10 show two examples. The distribution functions are shown in a $(L^2, 1-E)$-plot. For a fixed binding energy E, orbits with arbitrarily high angular momentum are not possible. Circular orbits have the highest amount of L^2 for a given E, and the heavy curve is the locus of all circular orbits; points 'below' it do not correspond to physical orbits. It can be shown [Veltmann (1966) or Paper I] that this boundary has the form

$$L^2=2[U(E)-E][U^{-2}(E)-1] \tag{57a}$$

with

$$U(E)=\sqrt[3]{E+\sqrt{E^2+1/27}}+\sqrt[3]{E-\sqrt{E^2+1/27}}. \tag{57b}$$

The shape of the distribution function is depicted by isoprobability contours. The different character of radial and tangential clusters are evident when comparing the contours that are drawn in full in both figures. Tangential clusters concentrate their orbits towards the boundary, where the circular orbits lie (this effect becomes evidently stronger with more negative q). It is clearly seen that the distribution function can vary appreciably for a fixed mass density and a fixed velocity dispersion, which are completely determined by the parameter q. The parameters n and a model the degeneracy. The higher the value of n, the less the 'perturbed' model differs from the

'unperturbed' one. This is a consequence of the fact that for high n, (52) is satisfied to high order. Whence, the greatest differences should occur for $n=2$. A comparison of both figures shows that a positive a tends to enhance the radial features of the model for the radial orbits (located close to the E-axis), and enhances the tangential features of the model for the more circular orbits (close to the boundary of the model). The orbits which lie 'in between' those two extremes are

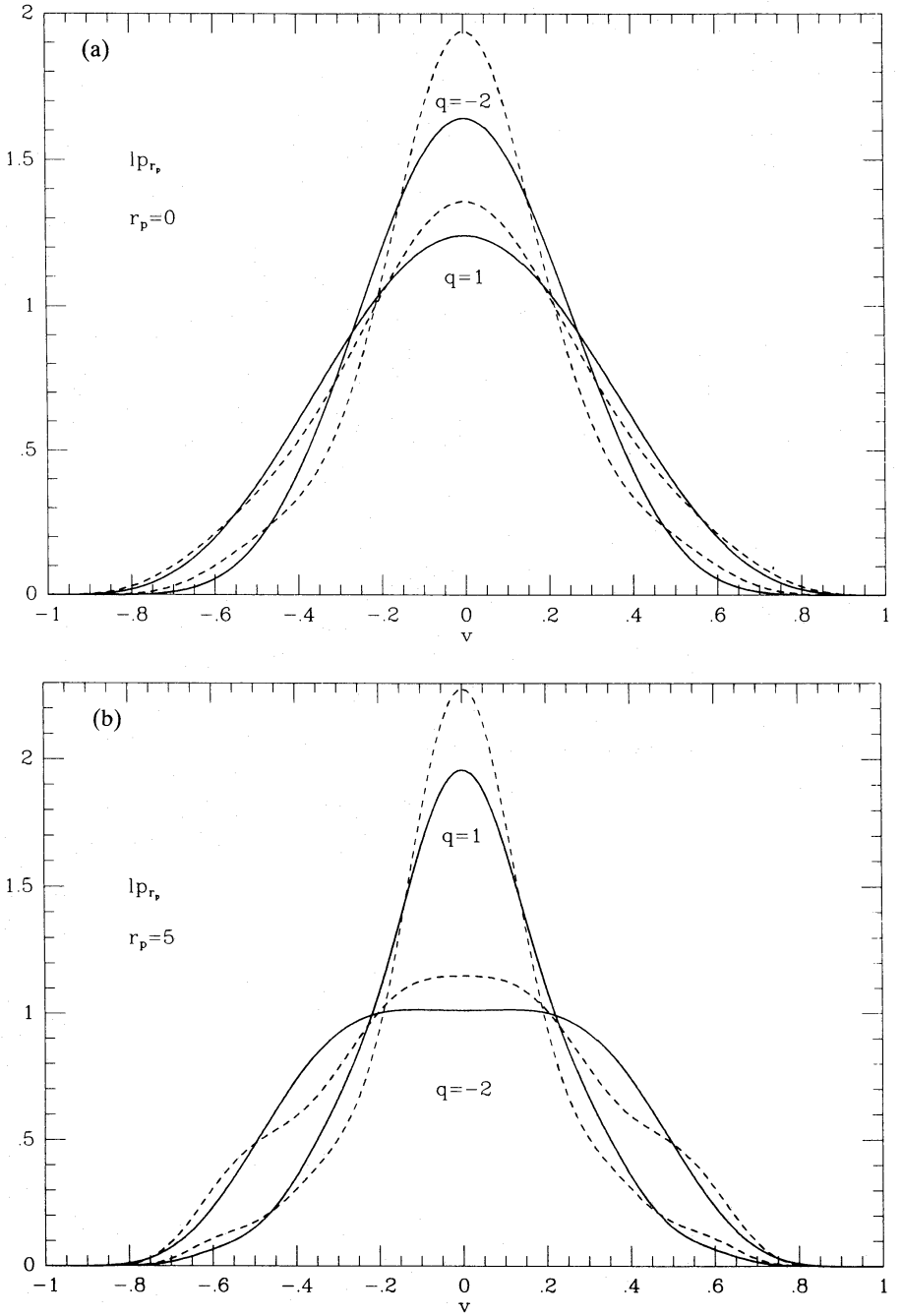

Figure 11. (a) Line profiles at the centre for four models. The two 'lower ones' are compatible with a $q=1$ radial model (in full and dashed) while the two 'higher ones' (in full and dashed) correspond to a $q=-2$ tangential model. The values of the other parameters (a and n) and their correspondence with line type are the same as in Figs 9 and 10. (b) Line profiles at the edge for four models. The two 'higher ones' are compatible with a $q=1$ radial model (in full and dashed) while the two 'lower ones' (in full and dashed) correspond to a $q=-2$ tangential model. The values of the other parameters (a and n) and their correspondence with line type are the same as in Figs 9 and 10.

depopulated. The parameters are chosen so that this effect is nearly maximum. This can be seen in Fig. 9 at the dip in the 3.E-6-contour. Higher values for a will cause the model to develop a negative distribution function there.

Essentially the same conclusions can be drawn from Fig. 11(a) and (b), where the corresponding line profiles are shown, both for small radius and at the edge. Again there is considerable difference between the 'perturbed' and the 'unperturbed' profiles: extreme radial or tangential orbits exclusively contribute either to the peak or the tail of the line profile, depending on whether we look into the centre or through the edges of the cluster. We clearly see that for larger a more weight is being assigned to the extreme orbits, while the ubiquitous intermediate types (around $v=0.5$) are depopulated. Those effects can be as large as 20 per cent. Taking into account that a rather extreme case is considered here, we can expect typical deviations from some standard line profile of the order of 10 per cent.

5 Conclusions

The results of this paper are mainly twofold. On the one hand, Section 3 shows the importance of considering completely analytical models which are sufficiently rich to illustrate all the important features of an anisotropic spherical cluster, including energy distribution, distribution of transverse motions, energy balance and virial theorem. The proposed models are members of a physically well-defined family; macroscopically they are the same objects (e.g. mass density and potential are fixed by the Plummer law). The internal dynamics, however, differ considerably, and various options can be chosen by tuning only a few parameters, of which q (see Section 3.2) is the most important. As a consequence, they can provide the initial conditions for n-body simulations when it is important to isolate the effects of different internal structure, without altering the overall physics [mass density or even velocity dispersions (in Section 4) are invariant].

The stability of the models is probably guaranteed, with a possible exception for the most radial models. It can be shown rigorously, using Antonov's (1962) criterion that all these models are stable with respect to radial perturbations, with the only exception of the $q=2$ model, which does not satisfy Antonov's sufficient criterion. On the other hand, the radial models are more prone to non-radial instabilities. If we apply the Fridman & Polyachenko (1984) criterion:

$$\xi=\frac{T_R}{T_T/2}<\xi_c\approx 1.70\pm 0.25, \tag{58}$$

with T_R the kinetic energy in radial motions, we find, using (35), that

$$\xi=\frac{4}{4-q}, \tag{59}$$

and therefore

$$q<1.6\pm 0.35, \tag{60}$$

whence, the criterion is not decisive for the models with $q>1.3$. The others are stable according to this criterion. It must be noted though, that a recent update of the above criterion (Polyachenko 1985) tends to favour a higher value for ξ_c with less scatter. This would result in a narrower interval of possible unstable models, and it would lie closer to $q=2$. On the other hand, an N-body simulation (Barnes, private communication) indicates that the $q=2$ model is unstable.

As far as the real-world observations are concerned, the picture is evidently not so clear cut. The various assumptions which are inherent in an analytical treatment of this kind allow one only to draw conclusions which bear upon the generic feature of the model, for it is only too easy to

think of all kinds of effects that could blur the picture, e.g. aspherical structures are likely to be detected, or, in regions were stellar interactions can be important, even other dynamical assumptions which account for different stellar masses may be more appropriate. It is important at this point to stress that the assumptions made in this paper are possibly the simplest assumptions which can pretend to provide a framework to account for the existing observations.

It is clear from Section 4 that it is not possible to think of a distribution function as a quantity that can be determined by mass density and velocity dispersions alone, though it is difficult to assess quite generally the freedom in a distribution function that is compatible with the existing data.

Suppose we know both the mass density and the velocity dispersions. Then, in this specific formalism of the Plummer family, we know q, and within these strong restrictions, we get variations in the shape of the line profiles of the order of 20 per cent. This suggests that, for a given low-dimensional family of models, we are probably able to make sensible use of the information from the line profiles to fix a candidate distribution function.

Suppose we know the mass density accurately, but not the velocity dispersions, which means, in this formalism, that q is unknown. We don't know the line profiles either, because otherwise we would have known the velocity dispersions. We have seen, e.g. from Figs 8 and 9, that the compatible distribution functions differ considerably in this case, and it will be difficult to put forward one particular choice.

Suppose at last that we don't know for sure either the velocity dispersions or the mass density, as is unfortunately always the case. Then we can safely guess that almost every model (that belongs to the large class of models which do not violate obvious observational constraints) will be possible, in other words, the distribution function is almost completely indeterminate.

The main reason that the last and unfavourable case applies is our fundamental ignorance about the mass-to-light ratio M/L. This fact will continue to frustrate us, whether or not we determine line profiles. However, the line profiles add one, at least conceptually, important ingredient: their tails extend to the escape velocity $\sqrt{2\psi(r)}$. Moreover, there is no reason why some luminous matter should not move at escape velocity and dark matter would. Of course, we all know that the determination of the tails of the line profiles is so difficult and ill-defined that it's almost equivalent to a thought-experiment, but, at least, it *is* a clean handle on the potential.

Once the potential is known, we are almost done, because we then know the crucial quantity that determines the dynamics. We don't need to determine it extremely accurately though, because we need not in the first instance retrieve the mass density from it through Poisson's equation (which would be an ill-defined operation on an ill-defined quantity). If we want to determine distribution functions, we do so essentially for luminous matter for we measure velocities and line profiles of that component. But the magnitude of the potential is important, especially ψ_0 which helps to fix units and puts constraints on the possible values of M/L.

The rest of the dish is model-fitting, and it can be served in many flavours, e.g. once we decide about a clearly discernible luminous mass-density component $\varrho(r)$ and having at our disposal the approximate $\psi(r)$, we can start building models $\varrho(\psi, r)$ essentially in a way as described in Section 3. The velocity dispersions then allow us to rule out the larger part of the models ('fixing q') and the line profiles add the finishing touch.

Acknowledgments

The author wishes to thank P. Hut for his suggestion to produce this paper. The comments of J. Bahcall, S. Casertano, J. Goodman, D. Merritt and S. Tremaine are greatly appreciated. It is a pleasure to thank T. de Zeeuw for reading an early version of the manuscript. This research was supported in part by NSF Grant PHY-82-17352.

References

Antonov, A. V., 1962. *Vestnik Liningrad Univ.*, **19,** 96.
Binney, J. J., 1978. *Mon. Not. R. astr. Soc.*, **183,** 501.
Binney, J. J. & Mamon, G. A., 1982. *Mon. Not. R. astr. Soc.*, **200,** 361.
Bouvier, P., 1963. *Publs Obs. Genève,* **65,** 195.
Dejonghe, H., 1984. *Astr. Astrophys.*, **133,** 225.
Dejonghe, H., 1986. *Phys. Rep.*, **133,** Nos 3–4.
de Zeeuw, P. T., 1985. *Mon. Not. R. astr. Soc.*, **216,** 273.
Eddington, A. S., 1916. *Mon. Not. R. astr. Soc.*, **76,** 572.
Erdélyi, A., 1954. *Tables of Integral Transforms,* Vol. 1, McGraw-Hill, New York.
Fridman, A. M. & Polyachenko, V. L., 1984. *Physics of Gravitating Systems,* Vol. I, Springer-Verlag, New York.
Gradshteyn, I. S. & Ryzhik, I. M., 1980. *Table of Integrals, Series and Products,* Academic Press, New York.
Hunter, C., 1975. *Astr. J.*, **80,** 783.
Kuz'min, G. G. & Veltmann, Yu.-I. K., 1967. *Tartu astr. Obs. Teated,* **36,** 3.
Merritt, D., 1985. *Astr. J.*, **90,** 1027.
Osipkov, L. N., 1979. *Sov. Astr. Lett.*, **5,** 77.
Plummer, H. C., 1911. *Mon. Not. R. astr. Soc.*, **71,** 460.
Polyachenko, V. L., 1985. *Bureau of Rep. on Astr. of the Acad. of Sc. USSR, Astr. Circular 1405, reprint CITA.*
Richstone, D. O. & Tremaine, S., 1984. *Astrophys. J.*, **286,** 27.
Tonry, J. L., 1983. *Astrophys. J.*, **266,** 58.
Veltmann, Yu.-I. K., 1965. *Tartu astr. Obs. Teated,* **35,** 5.
Veltmann, Yu.-I. K., 1966. *Tartu astr. Obs. Teated,* **35,** 345.

Appendix A: The moments of the line profiles

In this appendix we will calculate the nth moment of the observed radial velocity profile. We start with a few more definitions.

We define the moments of the distribution function $F(E, L)$ as

$$\mu_{2n,2m,2l}=M\int\int\int F(E,L)v_r^{2n}v_\varphi^{2m}v_\theta^{2l}\,dv_r\,dv_\varphi\,dv_\theta, \tag{A1}$$

were the integration ranges over all possible velocities. The odd moments are zero. We never need to be concerned with the higher moments with respect to $v_\theta (l\geq 2)$, as argued in 3.5, and it can be proved (Paper I) that

$$\mu_{2n,2m,0}=\frac{1}{\pi}\frac{2^{m+n}\Gamma(n+\tfrac{1}{2})\Gamma(m+\tfrac{1}{2})}{\Gamma(m+1)\Gamma(m+n)}\int_0^\psi(\psi-\psi')^{m+n-1}D_{r_2}^m[r^{2m}\varrho(\psi',r)]\,d\psi'. \tag{A2}$$

It can be seen that the special cases given in (10) and (11) relate to this more general notation through

$$\varrho\sigma_r^2=\mu_{2,0,0},\qquad \varrho\sigma_\varphi^2=\varrho\sigma_\theta^2=\mu_{0,2,0}=\mu_{0,0,2} \tag{A3}$$

and

$$\varrho\tau_{rr}^4=\mu_{4,0,0}, \tag{A4a}$$

$$\varrho\tau_{r\varphi}^4=\varrho\tau_{r\theta}^4=\mu_{2,2,0},\qquad \varrho\tau_{\varphi\theta}^4=_{0,2,2}, \tag{A4b}$$

$$\varrho\tau_{\varphi\varphi}^4=\varrho\tau_{\theta\theta}^4=\mu_{0,4,0}=\mu_{0,0,4}. \tag{A4c}$$

The moments of the projected velocity distribution along the line-of-sight at a particular point (r_p, z) in space are

$$\mu_{2n}=\left(\frac{z}{r}\mu_{.,0,0}+\frac{r_p}{r}\mu_{0,.,0}\right)^{2n}, \tag{A5}$$

which is a shorthand notation to stress that the general term of this binomial formula equals

$$\binom{2n}{2i}\left(\frac{z}{r}\right)^{2(n-i)}\left(\frac{r_p}{r}\right)^{2i}\mu_{2(n-i),2i,0}. \tag{A6}$$

We further define

$$\mu'_{n,m,0}=\mu_{2n,2m,0}\binom{2n}{2m}\Big/\binom{n}{m} \tag{A7}$$

and find, after substituting (A2) and relabelling of the indices

$$\mu'_{n-i,i,0}=\frac{1}{\sqrt{\pi}}\frac{2^n\Gamma(n+\tfrac{1}{2})}{\Gamma(n)\,\Gamma(i+1)}\int_0^{\psi}(\psi-\psi')^{n-1}D^i_{r_2}[r^{2i}\varrho(\psi',r)]\,d\psi'$$

which can be written more conveniently in complex form

$$\mu'_{n-i,i,0}=\frac{1}{\sqrt{\pi}}\frac{2^n\Gamma(n+\tfrac{1}{2})}{\Gamma(n)}\frac{1}{2\pi i}\int_{\mathscr{C}(r^2)}\frac{dt}{t-r^2}\int_0^{\psi}(\psi-\psi')^{n-1}\,d\psi'\,t^i(t-r^2)^{-i}\varrho(\psi',t), \tag{A8}$$

with $\mathscr{C}(r^2)$ a counterclockwise integration contour around r^2.

The expression for μ_{2n} can be written in terms of the modified moments

$$\mu_{2n}=\left(\frac{z^2}{r^2}\mu'_{.,0,0}+\frac{r_p^2}{r^2}\mu'_{0,.,0}\right)^n \tag{A9}$$

or, with (A8),

$$\mu_{2n}=\frac{1}{\sqrt{\pi}}\frac{2^n\Gamma(n+\tfrac{1}{2})}{\Gamma(n)}\frac{1}{2\pi i}\int_{\mathscr{C}(r)}\frac{dt}{t-r^2}\int_0^{\psi}(\psi-\psi')^{n-1}d\psi'\left(\frac{z^2}{r^2}+\frac{r_p^2 t}{r^2(t-r^2)}\right)^n\varrho(\psi',t)$$

which effectively eliminates the factor r^{2n} in the denominator:

$$\mu_{2n}=\frac{1}{\sqrt{\pi}}\frac{2^n\Gamma(n+\tfrac{1}{2})}{\Gamma(n)}\frac{1}{2\pi i}\int_{\mathscr{C}(r^2)}\frac{dt}{t-r^2}\int_0^{\psi}(\psi-\psi')^{n-1}d\psi'\left(1+\frac{r_p^2}{(t-r^2)}\right)^n\varrho(\psi',t). \tag{A10}$$

The real form, if desired, is

$$\mu_{2n}=\frac{1}{\sqrt{\pi}}\frac{2^n\Gamma(n+\tfrac{1}{2})}{\Gamma(n)}\sum_{i=0}^{n}\binom{m}{i}\frac{r_p^{2i}}{i!}\int_0^{\psi}(\psi-\psi')^{n-1}\,D^i_{r^2}\varrho(\psi',r)\,d\psi'. \tag{A11}$$

Equations (A10) and (A11) are quite general expressions and do not depend on the specific functional form of $\varrho(\psi, r)$.

We now introduce the particular Plummer form (17) for $\varrho(\psi, r)$, which yields

$$\mu_{2n}=\frac{3}{4\pi^{3/2}}\frac{2^n\Gamma(n+\tfrac{1}{2})\,\Gamma(6-q)}{\Gamma(n+6-q)}[\psi(r)]^{n+5-q}\frac{1}{2\pi i}\int_{\mathscr{C}(r^2)}\frac{dt}{t-r^2}\left[1+\frac{r_p^2}{(t-r^2)}\right]^n(1+t)^{-q/2}, \tag{A12}$$

which must be integrated through the cluster with

$$\mu_p^{2n}(r_p)=\int_{r_p}^{+\infty}\frac{dr^2}{\sqrt{r^2-r_p^2}}\mu_{2n}(r), \tag{A13}$$

or, after changing variables from t to $v=t+r^2$ and r^2 to $u=(r^2-r_p^2)/(1+r_p^2)$:

$$\mu_p^{2n}(r_p)=\frac{3}{4\pi^{3/2}}\frac{\Gamma(n+\frac{1}{2})\Gamma(6-q)}{\Gamma(n+6-q)}\frac{2^n}{(1+r_p^2)^{n/2+2}}$$
$$\times\frac{1}{2\pi i}\int_{\mathscr{C}(0)}\frac{dv}{v^{n+1}}\int_0^{+\infty}\frac{du}{\sqrt{u}}(v+x^2)^n(1+u+v)^{-q/2}(1+u)^{(q-n-5)/2}, \tag{A14}$$

with

$$x^2=\frac{r_p^2}{1+r_p^2}. \tag{A15}$$

The projected velocity v_p ranges from $-\sqrt{2\psi(r_p)}$ to $+\sqrt{2\psi(r_p)}$. We can renormalize this velocity according to (45). Moreover, the zeroth moment $\mu_p^0(r_p)$ should be equal to the projected mass density (37) – which can easily be verified – and it is handy to normalize the moments further with respect to this projected mass density at a given radius r_p. We therefore define

$$\mu^{2n}(x^2)=\frac{1}{\pi}\frac{2^n}{(1+r_p^2)^{n/2+2}}\mu_p^{2n}(r_p) \tag{A16}$$

and find

$$\mu^{2n}(x^2)=\frac{3\Gamma(6-q)}{4\sqrt{\pi}}\frac{\Gamma(n+\frac{1}{2})}{\Gamma(n+6-q)}\frac{1}{2\pi i}\int_{\mathscr{C}(0)}\frac{dt}{t^{n+1}}\int_0^{+\infty}\frac{du}{\sqrt{u}}(t+x^2)^n(1+u+t)^{-q/2}(1+u)^{(q-n-5)/2}. \tag{A17}$$

These moments all refer to line profiles with a span ranging over the normalized velocities $v\in[-1,+1]$ and which cover a unit area. We can obtain a computable form for (A17) by first expanding the nth power in the integrand

$$\mu^{2n}(x^2)=\frac{3\Gamma(6-q)}{4\sqrt{\pi}}\frac{\Gamma(n+\frac{1}{2})}{\Gamma(n+6-q)}\sum_{i=0}^{n}\binom{n}{i}x^{2i}$$
$$\times\frac{1}{2\pi i}\int_{\mathscr{C}(0)}\frac{dt}{t^{i+1}}\int_0^{+\infty}\frac{du}{\sqrt{u}}(t+x^2)^n(1+u+t)^{-q/2}(1+u)^{(q-n-5)/2},$$

yielding a polynomial in x^2, and then turn the contour back into derivatives, leading to

$$\mu^{2n}(x^2)=\frac{3\Gamma(6-q)}{4\sqrt{\pi}}\frac{\Gamma(n+\frac{1}{2})}{\Gamma(n+6-q)}\sum_{i=0}^{n}\binom{n}{i}\frac{(-x^2)^i}{i!}\frac{\Gamma(\frac{1}{2}q+i)}{\Gamma(\frac{1}{2}q)}\int_0^{+\infty}\frac{du}{\sqrt{u}}\frac{1}{(1+u)^{i+(n+5)/2}},$$

which is only a valid operation for $0<q\leq 2$, or

$$\mu^{2n}(x^2)=\tfrac{3}{4}\Gamma(6-q)\frac{\Gamma(n+\frac{1}{2})}{\Gamma(n+6-q)}\frac{\Gamma(\frac{1}{2}n+2)}{\Gamma(\frac{1}{2}n+\frac{5}{2})}{}_3F_2(-n,\tfrac{1}{2}q,\tfrac{1}{2}n+2;1,\tfrac{1}{2}n+\tfrac{5}{2};x^2), \tag{A18}$$

valid for all $q\leq 2$ by analytic continuation. It is easily verified that the special cases $n=0$, 1, 2 reduce to (37), (43) and (44) by taking (A16) into account.

Appendix B: The line profiles

We will derive here an expression for the normalized line profiles as a function of normalized

velocity. We start with (A17) which gives the $2n$th normalized moment:

$$\mu^{2n}=\frac{3}{4\sqrt{\pi}}\Gamma(6-q)\frac{\Gamma(n+\tfrac{1}{2})}{\Gamma(n+6-q)}\frac{1}{2\pi i}\int_{\mathscr{C}(0)}\frac{dt}{t}\int_0^{+\infty}\frac{du}{\sqrt{u}}\frac{(1+u)^{(q-5)/2}}{(1+u+t)^{q/2}}\frac{(1+x^2/t)^n}{(1+u)^{n/2}}. \tag{B1}$$

The integrand, considered as a function of t, has a pole of $(n+1)$-th order at $t=0$, in general a branch point at $t=-1-u$ and a branch cut which we choose here as the part of the negative real axis to the left of $-1-u$. A transformation from t to $(1+t)/(1+u)$ transforms the cut into the entire negative real axis and the integral equals

$$\mu^{2n}=\frac{3}{4\sqrt{\pi}}\Gamma(6-q)\frac{\Gamma(n+\tfrac{1}{2})}{\Gamma(n+6-q)}\frac{1}{2\pi i}\int_{\mathscr{C}(1)}\frac{dt}{t^{q/2}(t-1)}\int_0^{+\infty}\frac{du}{\sqrt{u}}\frac{[\![1+[x^2/(t-1)(1+u)]]\!]^n}{(1+u)^{5/2+n/2}}. \tag{B2}$$

Standard methods for deforming the contour $\mathscr{C}(1)$ towards the branch cut lead to

$$\mu^{2n}=\frac{3}{4\pi^{3/2}}\Gamma(6-q)\sin\frac{\pi q}{2}\int_0^{+\infty}\frac{dt}{t^{q/2}(1+t)}\int_0^{+\infty}\frac{du}{\sqrt{u}(1+u)^{5/2}}\frac{\Gamma(n+\tfrac{1}{2})}{\Gamma(n+6-q)}\alpha^n, \tag{B3}$$

with

$$\alpha=\frac{1}{\sqrt{1+u}}\left[1-\frac{x^2}{(1+t)(1+u)}\right], \tag{B4}$$

and the additional restriction that $0\leq q\leq 2$.

We can now easily recover the Laplace transform $\mathscr{LP}(s)$ of $\mathrm{lp}_{r_p}(v^2)$ with the known relation

$$\mathscr{LP}(s)=\sum_{n\geq 0}\frac{\mu^{2n}}{n!}(-s)^n. \tag{B5}$$

Substitution of (B3) into (B5) gives

$$\mathscr{LP}(s)=\frac{3}{4\pi}\sin\frac{\pi q}{2}\int_0^{+\infty}\frac{dt}{t^{q/2}(1+t)}\int_0^{+\infty}\frac{du}{\sqrt{u}(1+u)^{5/2}}{}_1F_1(\tfrac{1}{2};6-q;-\alpha s), \tag{B6}$$

or,

$$\mathscr{LP}(s)=\frac{3}{4\pi}\sin\frac{\pi q}{2}\int_0^{+\infty}\frac{dt}{t^{q/2}(1+t)}\int_0^{+\infty}\frac{du}{\sqrt{u}(1+u)^{5/2}}\exp(-\tfrac{1}{2}\alpha s)(\alpha s)^{(q-6)/2}M_{(q-5)/2,(5-q)/2}(\alpha s), \tag{B7}$$

with $M_{\lambda,\mu}(z)$ the Whittaker function [see e.g. Gradshteyn & Ryzhik (1980)]. The s-part of the Laplace transform (B7) happens to have a simple original [see Erdélyi (1954) p. 293, 5.20(1)] and we find finally

$$\mathrm{lp}_{r_p}(v)=\frac{3}{4\pi^{3/2}}\frac{\Gamma(6-q)}{\Gamma(11/2-q)}\sin\frac{\pi q}{2}\iint_{\alpha\geq v^2}\frac{dt\,du}{t^{q/2}(1+t)\sqrt{u}(1+u)^{5/2}\sqrt{\alpha}}\left(1-\frac{v^2}{\alpha}\right)^{9/2-q}, \tag{B8}$$

expressed as a probability distribution in v (not in v^2). Equation (B8) as such is still rather unwieldy for practical purposes. The special case $v=0$ however, is considerably easier:

$$\mathrm{lp}_{r_p}(0)=\frac{3}{4\pi^{3/2}}\frac{\Gamma(6-q)}{\Gamma(11/2-q)}\sin\frac{\pi q}{2}\int_0^{+\infty}\frac{dt}{t^{q/2}(1+t)}\int_0^{+\infty}\frac{(1+u)^{1/4}du}{\sqrt{u}(1+u)^{5/2}}\frac{1}{\sqrt{1-[x^2/(1+t)(1+u)]}}. \tag{B9}$$

It can be developed in powers of x^2 and readily integrated, resulting in

$$\mathrm{lp}_{r_p}(0)=\frac{3}{4}\frac{\Gamma(6-q)\,\Gamma(7/4)}{\Gamma(11/2-q)\,\Gamma(9/4)}\,{}_3F_2(1/2,1/2q,7/4;1,9/4;x^2). \tag{B10}$$

Appendix C: Asymptotic forms for the line profiles

The line profiles can also be calculated with a more straightforward algorithm which is simply the explicit integration over velocity space and through the cluster. This method is definitely not able to produce more elegant results than the method described in Appendix B, but it is rather elegant for obtaining the asymptotic expressions we need in order to fit the tails of lp_{r_p}.

It is useful to consider the isotropic and anisotropic case separately. The former case evidently can be dealt with more completely than the latter.

C.1 ISOTROPIC CASE

At every point in the isotropic cluster we can direct one of the velocity axes, say the v_x-axis, parallel with the line-of-sight. If we switch to polar coordinates in the (v_y, v_z)-plane, one of the integrations can be performed easily. We find

$$dv_p\iint F\,dv_y\,dv_z=2\pi\,dv_p\int_0^{\psi-v_p^2/2}F(\psi-\tfrac{1}{2}v_p^2-t)\,dt \tag{C1}$$

so that the line profile is given by

$$lp_{r_p}(v_p)=4\pi\int_{r_p^2}^{+\infty}\frac{r\,dr}{\sqrt{r^2-r_p^2}}\int_0^{\psi(r)-v_p^2/2}F[\psi(r)-\tfrac{1}{2}v_p^2-t]\,dt. \tag{C2}$$

The integral (C1) is easily evaluated in case of the isotropic Plummer model (16). We find

$$\frac{3\times 2^{11/2}}{63\pi^2}(\psi-\tfrac{1}{2}v_p^2)^{9/2}. \tag{C3}$$

The integral with respect to r in (C2) is more elaborate. After substitution of

$$\psi_p=(1+r_p^2)^{-1/2}, \tag{C4}$$

we find

$$\mathrm{lp}_{r_p}(v_p)=\frac{3\times 2^{13/2}}{63\pi^2}\psi_p(\psi_p-\tfrac{1}{2}v_p^2)^5\int_0^1\frac{u^{9/2}[\tfrac{1}{2}v_p^2+(\psi_p-\tfrac{1}{2}v_p^2)\,u]^{-2}\,du}{\sqrt{1-u}\sqrt{\psi_p+\tfrac{1}{2}v_p^2+(\psi_p-\tfrac{1}{2}v_p^2)\,u}}. \tag{C5}$$

Asymptotically, in the limit $\tfrac{1}{2}v_p^2\to\psi_p$, we get the expression for the tails of the line profile:

$$\mathrm{lp}_{r_p}(v_p)\approx\frac{3}{4\pi}\psi_p^{-3/2}(\psi_p-\tfrac{1}{2}v_p^2)^5, \tag{C6}$$

or, in dimensionless units (as defined in 3.6):

$$\mathrm{lp}_{r_p}(v)=\frac{3}{2^{3/2}}(1-v^2)^5+O[(1-v^2)^6]. \tag{C7}$$

C.2 ANISOTROPIC CASE

We can always direct the v_θ-axis perpendicular to the line-of-sight. This enables us to integrate over all v_θ, but the existing symmetry does not allow us any integration without using the

functional form of the distribution function. We find at best

$$\mathrm{lp}_{r_p}(v_p)=2\int_{r_p^2}^{+\infty}\frac{r\,dr}{\sqrt{r^2-r_p^2}}\int_{v_r=(r/z)v_p-(r_p/z)v_\psi}dv_\varphi\int dv_\theta\,F(E,L), \tag{C8}$$

where $F(E, L)$ is given in (19–20). We consider two cases.

C.2.1 Small r_p

The dominant contribution to the tail comes from stars with radial velocities close to the escape velocity. Angular momentum is then small and we approximate the distribution function by

$$F(E,L)\approx\frac{3}{2(2\pi)^{5/2}}\frac{\Gamma(6-q)}{\Gamma(9/2-q)}E^{7/2-q}, \tag{C9}$$

which is effectively isotropic. We can now go through the same analysis as in 1, and we find

$$\mathrm{lp}_{r_p}(v)=\frac{3}{2^{3/2}}(1+r_p^2)^{q/2}(1-v^2)^{5-q}+O[(1-v^2)^{6-q}]. \tag{C10}$$

C.2.2 Large r_p

The high-velocity stars we observe here are exclusively high angular momentum stars. The distribution function can be approximated by

$$F(E,L)\approx\frac{3}{\pi^{5/2}}\frac{2^{(q-7)/2}\Gamma(6-q)}{\Gamma(9/2-\frac{1}{2}q)\Gamma(1-\frac{1}{2}q)}E^{(7-q)/2}L^{-q}. \tag{C11}$$

The integration over v_θ ranges from $-\sqrt{2\psi-(v_r^2+v_\varphi^2)}$ to $\sqrt{2\psi-(v_r^2+v_\varphi^2)}$ and is found to result in

$$\frac{3}{\pi^2}\frac{2^{4-q/2}\Gamma(6-q)}{\Gamma(5-\frac{1}{2}q)\Gamma(1-\frac{1}{2}q)}[\psi-\tfrac{1}{2}(v_r^2+v_\varphi^2)]^{4-q/2}|v_\varphi|^{-q}, \tag{C12}$$

in the limit for v_φ approaching escape velocity. The integration over v_φ ranges over the interval that lies within the two values

$$v_\varphi=\frac{r_p}{r}v_p\pm\frac{z}{r}\sqrt{2\psi-v_p^2}.$$

We find after some algebra

$$\mathrm{lp}_{r_p}(v_p)\approx2\int_{r_p^2}^{+\infty}\frac{r\,dr}{\sqrt{r^2-r_p^2}}\frac{3}{(2\pi)^{3/2}}\frac{2^{q/2-1}\Gamma(6-q)}{\Gamma(11/2-\frac{1}{2}q)\Gamma(1-\frac{1}{2}q)}r_p^{-q}|v_p|^{-q}(\psi_p-\tfrac{1}{2}v_p^2)^{(9-q)/2}. \tag{C13}$$

This type of integral is again analogous to the isotropic case. In dimensionless units, it evaluates as

$$\mathrm{lp}_{r_p}(v)=\frac{3}{2^{3/2}}\frac{\Gamma(6-q)}{\Gamma(6-\frac{1}{2}q)\Gamma(1-\frac{1}{2}q)}\left(\frac{r_p^2}{1+r_p^2}\right)^{-q/2}(1-v^2)^{5-q/2}|v|^{-q}+O[(1-v^2)^{6-q/2}]. \tag{C14}$$